Travelling wave solutions of the perturbed mKdV equation that represent traffic congestion

Travelling wave solutions of the perturbed mKdV equation that represent traffic congestion

L. Hattam*

February, 2018

Abstract

A well-known optimal velocity (OV) model describes vehicle motion along a single lane road, which reduces to a perturbed modified Korteweg-de Vries (mKdV) equation within the unstable regime. Steady travelling wave solutions to this equation are then derived with a multi-scale perturbation technique, where the travelling wave propagation coordinate depends upon slow and fast variables. The leading order solution in the hierarchy is then written in terms of these multi-scaled variables. At the following order, a system of differential equations is highlighted that govern the slowly evolving properties of the leading solution. Next, it is shown that the critical points of this system signify travelling waves without slow variation. As a result, a family of steady waves with constant amplitude and period are identified. When periodic boundary conditions are satisfied, these solutions' parameters, including the wave speed, are associated with the driver's sensitivity, $\hat{a}$, which appears in the OV model. For some given $\hat{a}$, solutions of both an upward and downward form exist, with the downward type corresponding to traffic congestion. Numerical simulations are used to validate the asymptotic analysis and also to examine the long-time behaviour of our solutions.

1 Introduction

To minimise congestion it is necessary to understand traffic behaviour, which has led to many traffic related studies with varied perspectives. Nagatani (2002) has given an overview of the different methods that analyse vehicle motion. In general, these techniques can be classified as either a macroscopic or a microscopic approach.

From a macroscopic viewpoint, Lighthill and Whitham (1955) and Richards (1956) derived a first order nonlinear partial differential equation to characterise traffic density. These workings are now known as LWR theory, however the limitations of this analysis were highlighted by Daganzo (1995). Also, Daganzo (1995) discussed certain higher order models that were extensions of this LWR theory. Again, some model failings were identified, including the appearance of 'wrong-way travel'. Zhang (1998) later proposed an alternative higher order model without this defect.

Another option is the application of a microscopic model that describes driven-diffusive-systems, such as the KLS model (see Katz et al. (1983) and Katz et al. (1984)). For instance, Wang et al. (2014) used

*Department of Mathematics and Statistics, University of Reading, Whiteknights, Reading, UK

this method to study a vehicle system with multiple lanes. Monte-Carlo simulations and mean field theory were then utilised to establish the traffic dynamics.

The following optimal velocity (OV) model is also an example of a microscopic approach,

$$\frac{d^2x_j}{dt^2} = \hat{a}\left(V(\Delta x_j(t)) - \frac{dx_j}{dt}\right), \tag{1}$$

where $x_j(t)$ is the position of car j at time t, $\Delta x_j = x_{j+1} - x_j$ is car j's headway (the distance between car j and car $j+1$), V is the car's optimal velocity, $j = 0, 1, 2, \ldots, N$ for N cars on the road and $\hat{a}$ is the driver's sensitivity, which is equal to the inverse of the delay time of the driver and vehicle. This equation was derived by Newell (1961) and Bando et al. (1995) to describe vehicle behaviour on a single lane road. In particular, it ensures that car j accelerates or decelerates in order to achieve a safe distance between itself and the preceding vehicle. The traffic model (1) can be rewritten in terms of the headway such that

$$\frac{d^2\Delta x_j}{dt^2} = \hat{a}\left(V(\Delta x_{j+1}(t)) - V(\Delta x_j(t)) - \frac{d\Delta x_j}{dt}\right). \tag{2}$$

As well, Bando et al. (1995) proposed an optimal velocity function, which is of the form

$$V(\Delta x_j(t)) = \tanh(\Delta x_j - h_c) + \tanh(h_c), \tag{3}$$

where h_c is the perceived safe headway distance. This function satisfies the necessary conditions of $V(\Delta x_j(t) = 0) = 0$, V being bounded and $V(h^{'}) < V(h_c)$ $(V(h^{''}) > V(h_c))$ for $h^{'} < h_c$ $(h^{''} > h_c)$. By applying linear stability analysis to (2), a neutral stability line with a critical point is obtained. This line signifies the boundary between two stability regions referred to as metastable and unstable. See Ge et al. (2005) for further detail.

Muramatsu and Nagatani (1999) reduced (2) to a perturbed Korteweg-de Vries (KdV) equation within the metastable zone using nonlinear theory. This was the KdV equation with higher order correction terms. They then numerically identified traffic solitons propagating over open boundaries, which eventually dissolved. This behaviour is expected within this stability regime since all solutions should tend to the uniform headway. Hattam (2017) studied this problem with periodic boundaries, where cnoidal waves were shown to exist that represented traffic congestion. These solutions were derived using modulation theory and then validated with numerical simulations. Again, these density waves disappeared after some time.

In contrast, solutions corresponding to the unstable region were identified by Komatsu and Sasa (1995). Beginning with (2) close to the critical point on the neutral stability line, they derived a perturbed modified KdV (mKdV) equation. The leading order solution to this equation was written in terms of Jacobi elliptic functions that were dependent upon the elliptic modulation term $m \in [0, 1]$. When $m = 1$, this solution became the kink soliton, which exhibits the start/stop motion representative of a traffic jam. Komatsu and Sasa (1995) then applied perturbation analysis to seek steady travelling wave solutions of the mKdV traffic model. They established that this solution type only existed when the wave modulus m remained constant and consequently, the wave amplitude and period were fixed. A condition for m as some constant was next found in terms of integral constraints, which then determined

the relationship between m and the wave speed. They referred to the travelling wave solutions with $m = 1$ as deformed kink solitons. Otherwise, for constant $m \neq 1$, they were labelled deformed periodic solitons.

Here, a multi-scale perturbation technique is applied to the perturbed mKdV equation to also identify steady travelling wave solutions. This approach is an adaptation of the method outlined by Hattam and Clarke (2015) for the steady forced KdV-Burgers equation. Solutions of a similar form to the deformed periodic solitons found by Komatsu and Sasa (1995) are highlighted, which satisfy periodic boundaries. Komatsu and Sasa (1995) proposed that this solution type was always unstable and only deformed kink solitons were observed numerically. The stability of our periodic waves is investigated here.

Such studies as Zhu and Dai (2008) and Zheng et al. (2012) have numerically examined OV traffic models within the unstable zone, where periodic boundary conditions were imposed. The long-time behaviour was analysed, which revealed solutions that were indicative of mKdV dynamics as kink-like waves appeared. Moreover, Li et al. (2015) performed numerical simulations over large time intervals of an OV model that described a two-lane system with periodic boundaries. As well, this model was transformed into a perturbed mKdV equation near to the critical point. The numerical results corresponding to this region uncovered steady periodic travelling wave solutions with constant amplitude, mean height and period. Hence, these numerical findings suggest stable periodic solutions to the OV traffic system do propagate within this unstable regime. Therefore, additional work is needed to determine the link between the numerical results and the nonlinear theory.

The focus of this paper is the derivation of steady travelling wave solutions to (2) and then the analysis of their long-time dynamics. In Section 2, (2) is reduced to a perturbed mKdV equation and then steady travelling wave solutions are determined using a multi-scale perturbation method in Section 3. The leading order solution is obtained in terms of Jacobi elliptic functions that depend upon slow and fast variables. At the next order, a dynamical system governing the slow variation of the leading order solution is identified. Then, in Section 4, the fixed points of this system are shown to represent a family of steady travelling waves that do not slowly vary. This set of solutions have fixed amplitude, mean height and period. Also, the relations between the solution parameters, the wave speed and the driver's sensitivity are established due to implementing periodic boundary conditions. Lastly, in Section 5, the highlighted periodic asymptotic solutions are compared with numerical results and their long-time behaviour is studied.

2 Traffic Flow Model

We now outline how the OV model (2) is transformed into a perturbed mKdV equation. This then becomes the steady perturbed Gardner equation when we seek steady travelling wave solutions.

Firstly, Bando et al. (1995) deduced for the system (2), the linear stability criterion

$$\hat{a} \geq \hat{a}_s = 2V^{'}(h), \tag{4}$$

where h is the uniform headway ($\Delta x_j(t) = h$ is the steady solution of (2) for h is some constant). When (4) is met, the steady state of $\Delta x_j(t) = h$ is stable. The curve defined by $\hat{a} = \hat{a}_s$ is the 'neutral stability

line', which indicates the onset of instability. The maximum point of this curve occurs when $h = h_c$ and $\hat{a} = \hat{a}_c = 2V^{'}(h_c)$, which means $V^{''}(h_c) = 0$. The region neighbouring this point is where (2) reduces to the perturbed mKdV equation.

Now, we set

$$\bar{x} = \epsilon(j + V^{'}(h_c)t), \quad \bar{t} = \epsilon^3 \frac{V^{'}(h_c)}{6} t, \quad \epsilon^2 = (\hat{a}_c/\hat{a}) - 1, \quad 0 < \epsilon \ll 1, \tag{5}$$

and let

$$\Delta x_j(t) = h_c + \epsilon \sqrt{\frac{V'(h_c)}{\mid V'''(h_c) \mid}} R. \tag{6}$$

This change of variables is consistent with Ge et al. (2005).

As a result, (2) becomes

$$R_{\bar{t}} - R_{\bar{x}\bar{x}\bar{x}} + 3R^2 R_{\bar{x}} + \epsilon \left(3R_{\bar{x}\bar{x}} + \frac{3}{4} R_{\bar{x}\bar{x}\bar{x}\bar{x}} - \frac{1}{2} \partial_{\bar{x}\bar{x}}(R^3) - \xi (R^4)_{\bar{x}} \right) = 0, \tag{7}$$

where

$$\xi = \frac{1}{4} \sqrt{\frac{V'(h_c)}{\mid V'''(h_c) \mid^3}} V''''(h_c),$$

and $O(\epsilon^2)$ terms are ignored. This is a perturbed mKdV equation as ϵ is small. Note that $\xi = 0$ when V is defined using (3), however we assume that ξ is some constant in the following section so that the analysis is more general.

Since $\epsilon > 0$ and therefore $\hat{a} < \hat{a}_c$, the stability criterion (4) does not hold and the steady state of $\Delta x_j(t) = h_c$ is unstable. Thus, this is the unstable regime. As well, since $\epsilon \ll 1$, (7) is only valid within the vicinity of the point $(h = h_c, \hat{a} = \hat{a}_c)$.

Here, steady travelling wave solutions of (7) are sought. To identify this solution type, we set $\tilde{x} = \bar{x} - \omega \bar{t}$, where ω is the constant wave speed. As well, if

$$\sqrt{\omega} u = R + \sqrt{\frac{\omega}{3}}, \tag{8}$$

then (7) becomes

$$\lambda u_{\tilde{x}\tilde{x}\tilde{x}} - \gamma u^2 u_{\tilde{x}} + \nu u u_{\tilde{x}} + \epsilon G(u, \tilde{x}) = 0, \tag{9}$$

where

$$\lambda = 1, \quad \gamma = 3\omega, \quad \nu = 2\sqrt{3}\omega, \tag{10}$$

and

$$G(u, \tilde{x}) = -\left(3u_{\tilde{x}\tilde{x}} + \frac{3}{4} u_{\tilde{x}\tilde{x}\tilde{x}\tilde{x}} - \frac{\omega}{2} \partial_{\tilde{x}\tilde{x}} \left(\left(u - \frac{1}{\sqrt{3}} \right)^3 \right) - \xi \omega \sqrt{\omega} \left(\left(u - \frac{1}{\sqrt{3}} \right)^4 \right)_{\tilde{x}} \right). \tag{11}$$

The system (9) is the steady perturbed Gardner equation. The parameters λ, γ, ν have been introduced so that initially the analysis is generalised. Consequently, a general scheme is outlined to obtain solutions of any steady perturbed Gardner equation. Note that due to using (8), the coefficients of the first two nonlinear terms are now proportional to ω ($\nu/\gamma = 2/\sqrt{3}$). This becomes a necessary condition in Section 4 when highlighting certain solutions.

3 Perturbation Analysis

The modulation theory detailed by Hattam and Clarke (2015) for the steady perturbed KdV equation is now applied to (9). However, since an additional cubic nonlinear term must be considered, the modulation theory for the Gardner equation is also used, which was outlined by Kamchatnov et al. (2012). As a result of this perturbation analysis, a leading order solution to (9) is highlighted that varies with slow and fast variables. Then at the next order, equations are found that describe the slow evolution of this solution.

Myint and Grimshaw (1995) applied multi-scale analysis to the perturbed KdV equation, which was essentially the WKB approximation (see Wentzel (1926), Kramers (1926) and Brillouin (1926)). A steady form of this theory is used here. To begin, let

$$X = \epsilon\tilde{x}, \quad \theta_X = \frac{1}{\epsilon}k(X), \tag{12}$$

and

$$u(\tilde{x}) = u_0(\theta, X) + \epsilon u_1(\theta, X) + \epsilon^2 u_2(\theta, X) + O(\epsilon^3), \tag{13}$$

where X and θ are 'slow' and 'fast' variables respectively, and k is some function of X.

Subsequent to the change of variables (12) and using the approximation (13), (9) takes the form at first and second order

$$O(1) : \lambda k^2 u_{0,\theta\theta\theta} - \gamma u_0^2 u_{0,\theta} + \nu u_0 u_{0,\theta} = 0, \tag{14a}$$

$$O(\epsilon) : \lambda k^3 u_{1,\theta\theta\theta} - \gamma k\left(u_0^2 u_1\right)_\theta + \nu k(u_0 u_1)_\theta + g = 0, \tag{14b}$$

where

$$g(\theta, X) = G(\theta, X) + 3\lambda k^2 u_{0,\theta\theta X} - \gamma u_0^2 u_{0,X} + \nu u_0 u_{0,X} + 3\lambda k k_X u_{0,\theta\theta}. \tag{15}$$

The integration of (14a) gives

$$\frac{3\lambda k^2}{\gamma} u_{0,\theta\theta} = u_0^3 - \frac{3\nu}{2\gamma} u_0^2 + \frac{3}{\gamma}\hat{C}, \tag{16}$$

then multiplying (16) by $u_{0,\theta}$ and integrating, we arrive at

$$\frac{6\lambda k^2}{\gamma} u_{0,\theta}^2 = u_0^4 - \frac{2\nu}{\gamma} u_0^3 + \frac{12}{\gamma}\hat{C} u_0 + \frac{12}{\gamma}\hat{D}, \tag{17}$$

where $\hat{C}$ and $\hat{D}$ are integration constants. Next, let

$$Q(u_0) = u_0^4 - \frac{2\nu}{\gamma} u_0^3 + \frac{12}{\gamma}\hat{C} u_0 + \frac{12}{\gamma}\hat{D}, \tag{18}$$

where Q is a polynomial of order 4. Suppose that $a \le b \le c \le d$ are the roots of this polynomial, then

$$u_0^4 - \frac{2\nu}{\gamma} u_0^3 + \frac{12}{\gamma}\hat{C} u_0 + \frac{12}{\gamma}\hat{D} = Q(u_0) = (u_0 - a)(u_0 - b)(u_0 - c)(u_0 - d). \tag{19}$$

By expanding the righthand side of (19) and equating like terms, we find

$$\frac{2\nu}{\gamma} = a + b + c + d, \tag{20a}$$

$$\frac{12\hat{C}}{\gamma} = -(acd + abd + abc + bcd), \tag{20b}$$

$$\frac{12\hat{D}}{\gamma} = abcd, \tag{20c}$$

$$0 = bc + ac + cd + ab + bd + ad. \tag{20d}$$

So the equation parameters are dependent upon the roots a, b, c, d. As well, since $Q(u_0 = a, b, c, d) = 0$, then

$$a\hat{C} + \hat{D} = \frac{\nu a^3}{6} - \frac{\gamma a^4}{12}, \tag{21a}$$

$$b\hat{C} + \hat{D} = \frac{\nu b^3}{6} - \frac{\gamma b^4}{12}, \tag{21b}$$

$$c\hat{C} + \hat{D} = \frac{\nu c^3}{6} - \frac{\gamma c^4}{12}, \tag{21c}$$

$$d\hat{C} + \hat{D} = \frac{\nu d^3}{6} - \frac{\gamma d^4}{12}. \tag{21d}$$

Now, written in terms of these roots, (14a) has the well-known solution (see Kamchatnov et al. (2012))

$$u_0(\theta, X) = \frac{ce + d\,\mathrm{sn}^2\left(\beta(\theta - \theta_0); m\right)}{e + \mathrm{sn}^2\left(\beta(\theta - \theta_0); m\right)}, \tag{22}$$

where the function sn is the Jacobi elliptic function, $m \in (0, 1)$ is its elliptic modulus and

$$\frac{24\lambda\beta^2 k^2}{\gamma} = (a - c)(b - d), \tag{23a}$$

$$e = -\left(\frac{b - d}{b - c}\right), \tag{23b}$$

$$m^2 = \frac{(a - d)(b - c)}{(a - c)(b - d)}. \tag{23c}$$

The parameters $a, b, c, d, m, \theta_0, k, \beta$ are all dependent on the slow variable X. We denote the period of (22) in the θ direction by $2P$, where P is some constant, which means

$$P = K(m)/\beta. \tag{24}$$

The function $K(m)$ is the complete elliptic integral of the first kind. Note that if k is some constant function, then the period of (22) in terms of $\tilde{x}$ will be $2P/k = (2K(m))/\beta k$, where βk is given by (23a).

To ensure the next order solution, u_1, has the period $2P$, the periodicity conditions

$$\frac{1}{2P}\int_{\theta_1}^{\theta_2} g(\theta, X)d\theta = 0, \tag{25a}$$

$$\frac{1}{2P}\int_{\theta_1}^{\theta_2} g(\theta, X)u_0 d\theta = 0, \tag{25b}$$

are imposed, where $\theta_1 = -P+\theta_0$ and $\theta_2 = P+\theta_0$. These integral constraints are the result of integrating (14b) and $u_0\times$(14b) over the domain $\theta \in [\theta_1, \theta_2]$. Note that u_0 and its derivatives with respect to θ are assumed to be periodic over $\theta \in [\theta_1, \theta_2]$. The integral (25b) written in full, given (15), is

$$\frac{1}{2P}\int_{\theta_1}^{\theta_2} G u_0 d\theta + \frac{1}{2P} I_b = 0, \tag{26}$$

where

$$\begin{aligned} I_b &= \int_{\theta_1}^{\theta_2} \left(3\lambda(k^2 u_{0,\theta\theta X} + k k_X u_{0,\theta\theta}) - \gamma u_0^2 u_{0,X} + \nu u_0 u_{0,X}\right) u_0 d\theta \\ &= \partial_X \int_{\theta_1}^{\theta_2} \left(-\frac{3\lambda k^2}{2} u_{0,\theta}^2 - \frac{\gamma}{4} u_0^4 + \frac{\nu}{3} u_0^3\right) d\theta. \end{aligned} \tag{27}$$

Next, by manipulating $u_0\times$(16) and (17), it can be shown

$$\frac{3\gamma}{2P}\int_{\theta_1}^{\theta_2} u_0^4 d\theta = \frac{5\nu}{2P}\int_{\theta_1}^{\theta_2} u_0^3 d\theta - \frac{18\hat{C}}{2P}\int_{\theta_1}^{\theta_2} u_0 d\theta - 12\hat{D}, \tag{28a}$$

$$\frac{18\lambda k^2}{2P}\int_{\theta_1}^{\theta_2} u_{0,\theta}^2 d\theta = -\frac{\nu}{2P}\int_{\theta_1}^{\theta_2} u_0^3 d\theta + \frac{18}{2P}\hat{C}\int_{\theta_1}^{\theta_2} u_0 d\theta + 24\hat{D}. \tag{28b}$$

Combining these, gives

$$-\frac{18\lambda k^2}{2P}\int_{\theta_1}^{\theta_2} u_{0,\theta}^2 d\theta + \frac{1}{2P}\int_{\theta_1}^{\theta_2} (-3\gamma u_0^4 + 4\nu u_0^3) d\theta = -12\hat{D},$$

and therefore, (27) takes the form

$$\frac{1}{2P} I_b = -\hat{D}_X.$$

As well, the integral (25a) can be written, given (15),

$$\frac{1}{2P}\int_{\theta_1}^{\theta_2} G d\theta + \frac{1}{2P} I_a = 0, \tag{29}$$

where

$$\begin{aligned} I_a &= \int_{\theta_1}^{\theta_2} \left(3\lambda(k^2 u_{0,\theta\theta X} + k k_X u_{0,\theta\theta}) - \frac{\gamma}{3}(u_0^3)_X + \frac{\nu}{2}(u_0^2)_X\right) d\theta \\ &= \partial_X \int_{\theta_1}^{\theta_2} \left(-\frac{\gamma}{3} u_0^3 + \frac{\nu}{2} u_0^2\right) d\theta, \\ &= 2P\hat{C}_X, \end{aligned}$$

using (17).

Thus, the integral conditions (25) reduce to

$$\hat{C}_X = -\frac{1}{2P}\int_{\theta_1}^{\theta_2} G(\theta, X) d\theta, \tag{30a}$$

$$\hat{D}_X = \frac{1}{2P}\int_{\theta_1}^{\theta_2} G(\theta, X) u_0 d\theta. \tag{30b}$$

This system determines the slow variation of the leading order solution (22) for some given function $G(\theta, X)$. Therefore, (22) and (30) define solutions to any steady perturbed Gardner equation. Next, by applying the relevant equation parameters λ, γ, ν and the function G, unique solutions can be derived.

3.1 Application to the traffic flow model

So to locate steady travelling wave solutions of the traffic model (2), G is now defined by (11). Firstly,

$$\int_{\theta_1}^{\theta_2} G(\theta, X)d\theta = \frac{\omega k^2}{2}\left[3\left(u_0 - \frac{1}{\sqrt{3}}\right)^2 u_{0,\theta}\right]_{\theta_1}^{\theta_2} + \xi\omega\sqrt{\omega}k\left[\left(u_0 - \frac{1}{\sqrt{3}}\right)^4\right]_{\theta_1}^{\theta_2} = 0,$$

where $O(\epsilon)$ terms are ignored. Therefore, from (30a), $\hat{C}$ is some constant.

Next let us set $\hat{D}_X = \tilde{I}$, so that

$$\tilde{I} = \frac{1}{2P}\int_{\theta_1}^{\theta_2} G(\theta, X)u_0 d\theta.$$

Using (11) to define G, this integral becomes

$$\begin{aligned}
\tilde{I} &= -\frac{1}{2P}\int_{\theta_1}^{\theta_2} u_0\left(3k^2u_{0,\theta\theta} + \frac{3}{4}k^4u_{0,\theta\theta\theta\theta} - \frac{\omega}{2}k^2\partial_{\theta\theta}\left(\left(u_0 - \frac{1}{\sqrt{3}}\right)^3\right) - \xi\omega\sqrt{\omega}k\partial_\theta\left(\left(u_0 - \frac{1}{\sqrt{3}}\right)^4\right)\right)d\theta \\
&= -\frac{1}{2P}\int_{\theta_1}^{\theta_2}\left(3k^2u_0u_{0,\theta\theta} + \frac{3}{4}k^4u_0u_{0,\theta\theta\theta\theta} + \frac{\omega}{2}k^2u_{0,\theta}\partial_\theta\left(\left(u_0 - \frac{1}{\sqrt{3}}\right)^3\right) + \frac{\xi\omega\sqrt{\omega}}{5}k\partial_\theta\left(\left(u_0 - \frac{1}{\sqrt{3}}\right)^5\right)\right)d\theta \\
&= -\frac{1}{2P}\int_{\theta_1}^{\theta_2}\left(-3k^2u_{0,\theta}^2 + \frac{3}{4}k^4u_0u_{0,\theta\theta\theta\theta} + \frac{3\omega}{2}k^2u_{0,\theta}^2\left(u_0^2 - \frac{2}{\sqrt{3}}u_0 + \frac{1}{3}\right)\right)d\theta.
\end{aligned} \tag{31}$$

Hence, to write $\tilde{I}$ in closed form we must solve the integrals

$$\tilde{I}_1 = \frac{1}{2P}\int_{\theta_1}^{\theta_2} u_{0,\theta}^2 d\theta, \quad \tilde{I}_2 = \frac{1}{2P}\int_{\theta_1}^{\theta_2} u_0u_{0,\theta}^2 d\theta, \quad \tilde{I}_3 = \frac{1}{2P}\int_{\theta_1}^{\theta_2} u_0^2u_{0,\theta}^2 d\theta, \quad \tilde{I}_4 = \frac{1}{2P}\int_{\theta_1}^{\theta_2} u_0u_{0,\theta\theta\theta\theta} d\theta. \tag{32}$$

The computation of these integrals is outlined in the Appendix. Omitting these details here, (31) reduces to

$$\tilde{I} = k^2\left(\tilde{I}_1\left(3 - \frac{\omega}{2}\right) + \tilde{I}_2\left(-\frac{3\nu}{4\lambda} + \sqrt{3}\omega\right) + 3\tilde{I}_3\left(\frac{\gamma}{4\lambda} - \frac{\omega}{2}\right)\right), \tag{33}$$

where

$$\tilde{I}_1 = \frac{1}{\lambda k^2}\left(-\frac{\nu^2}{12\gamma}\alpha_2 + \left(\alpha_1 + \frac{\nu}{6\gamma}\right)\hat{C} + \frac{4}{3}\hat{D}\right), \tag{34a}$$

$$\tilde{I}_2 = \frac{\gamma}{6\lambda k^2}\left(\alpha_2\left(\frac{9\hat{C}}{2\gamma} - \frac{5\nu^3}{8\gamma^3}\right) + \alpha_1\left(\frac{6\hat{D}}{\gamma} + \frac{3\nu\hat{C}}{2\gamma^2}\right) + \frac{5\nu^2\hat{C}}{4\gamma^3} + \frac{\nu\hat{D}}{\gamma^2}\right), \tag{34b}$$

$$\tilde{I}_3 = \frac{\gamma}{6\lambda k^2}\left(\alpha_2\left(\frac{69\hat{C}\nu}{10\gamma^2} - \frac{7\nu^4}{8\gamma^4} + \frac{24\hat{D}}{5\gamma}\right) + \alpha_1\left(\frac{6\nu\hat{D}}{5\gamma^2} + \frac{21\nu^2\hat{C}}{10\gamma^3}\right) + \frac{35\nu^3\hat{C}}{20\gamma^4} + \frac{7\nu^2\hat{D}}{5\gamma^3} - \frac{54\hat{C}^2}{5\gamma^2}\right). \tag{34c}$$

The integrals α_1 and α_2 are defined and written in full in the Appendix.

4 Fixed Points

In Section 3, the leading order solution (22) of the traffic model (2) was obtained. Moreover, its slow variation was found to be governed by the system

$$\hat{C}_X = 0, \tag{35a}$$

$$\hat{D}_X = \tilde{I}, \tag{35b}$$

where $\tilde{I}$ is given by (33)-(34). The critical points of this system occur when $\hat{C}_X = \hat{D}_X = 0$, which suggests that $\tilde{I} = 0$ and $\hat{C}, \hat{D}$ are some constants at the fixed points ($\hat{C}$ is always constant). We now want to highlight these fixed point solutions. Firstly, it is shown that if $\hat{D}_X = 0$, the corresponding solutions will have constant wave amplitude, mean height and period. Then, by setting $\tilde{I} = 0$, a definition for the wave speed of the fixed point solutions is obtained.

Now, taking the derivative of (21a) with respect to X gives

$$\hat{D}_X = \frac{1}{6}\left(3a^2\nu - 2a^3\gamma - 6\hat{C}\right)a_X,$$

using $\hat{C}$ is some constant ($\hat{C}_X = 0$). Similarly, (21b)-(21d) take the form

$$\hat{D}_X = \frac{1}{6}\left(3b^2\nu - 2b^3\gamma - 6\hat{C}\right)b_X = \frac{1}{6}\left(3c^2\nu - 2c^3\gamma - 6\hat{C}\right)c_X = \frac{1}{6}\left(3d^2\nu - 2d^3\gamma - 6\hat{C}\right)d_X.$$

So, if $\hat{D}_X = 0$, then

$$a_X = b_X = c_X = d_X = 0. \tag{36}$$

As well, from (23c) it can be shown

$$\begin{aligned}\frac{2}{m}m_X =& a_X\left(\frac{1}{a-d} - \frac{1}{a-c}\right) + b_X\left(\frac{1}{b-c} - \frac{1}{b-d}\right)\\ &+ c_X\left(\frac{1}{a-c} - \frac{1}{b-c}\right) + d_X\left(\frac{1}{b-d} - \frac{1}{a-d}\right).\end{aligned}$$

Therefore, when $\hat{D}_X = 0$, (36) is satisfied, and therefore

$$m_X = 0. \tag{37}$$

Hence, the fixed point solutions of the system (35) (when $\hat{D}_X = 0$) correspond to the leading order solution (22) with constant wave modulus m and constant solution parameters a, b, c, d, β (since $m_X = a_X = b_X = c_X = d_X = 0$). So then, these particular steady travelling waves do not have slowly varying properties, which means their amplitude, mean height and period remain fixed. Therefore, they are of a similar form to the deformed periodic solitons detailed by Komatsu and Sasa (1995).

Next, it is necessary to outline the parameter space that corresponds to these fixed point solutions. Firstly, we set

$$\kappa_1 = \frac{\hat{C}}{\gamma} = \frac{\hat{C}}{3\omega}, \quad \kappa_2 = \frac{\hat{D}}{\gamma} = \frac{\hat{D}}{3\omega}, \tag{38}$$

where κ_1 and κ_2 are some constants since we know that ω is the constant wave speed and $\hat{C}, \hat{D}$ are constants (they are independent of X at the critical point). Also, the equation parameters λ and ν/γ are defined using (10). As a result, (18) is written

$$Q(z) = z^4 - \frac{4}{\sqrt{3}}z^3 + 12\kappa_1 z + 12\kappa_2. \tag{39}$$

Note that since a, b, c, d are determined by the four roots of (39) (which as a result defines e and m using (23b) and (23c)), then the quantities $\alpha_1(m, c, d, e)$ and $\alpha_2(m, c, d, e)$ are only dependent upon $\kappa_{1,2}$.

Now, rewriting (33) in terms of κ_1 and κ_2 gives

$$\tilde{I} = 3k^2\tilde{I}_1 + k^2\omega\left(-\frac{1}{2}\tilde{I}_1 + \frac{1}{4}(3\tilde{I}_3 - 2\sqrt{3}\tilde{I}_2)\right), \tag{40}$$

where

$$\tilde{I}_1 = \frac{\gamma}{k^2}\left(\alpha_1\kappa_1 - \frac{\alpha_2}{9} + \frac{\kappa_1}{3\sqrt{3}} + \frac{4\kappa_2}{3}\right),$$
$$\tilde{I}_2 = \frac{\gamma}{6k^2}\left(\alpha_1\left(\frac{3\kappa_1}{\sqrt{3}} + 6\kappa_2\right) + \alpha_2\left(\frac{9\kappa_1}{2} - \frac{5}{3\sqrt{3}}\right) + \frac{5\kappa_1}{3} + \frac{2\kappa_2}{\sqrt{3}}\right),$$
$$\tilde{I}_3 = \frac{\gamma}{6k^2}\left(\alpha_1\left(\frac{14\kappa_1}{5} + \frac{12\kappa_2}{5\sqrt{3}}\right) + \alpha_2\left(\frac{69\kappa_1}{5\sqrt{3}} + \frac{24\kappa_2}{5} - \frac{14}{9}\right) + \frac{14\kappa_1}{3\sqrt{3}} + \frac{28\kappa_2}{15} - \frac{54}{5}{\kappa_1}^2\right).$$

By setting $\tilde{I} = 0$ (refer to (40)) and rearranging, a definition for the constant wave speed is found as a function of κ_1, κ_2, $\alpha_1(m,c,d,e)$ and $\alpha_2(m,c,d,e)$, such that

$$\omega = -\frac{3\tilde{I}_1}{\frac{1}{4}(3\tilde{I}_3 - 2\sqrt{3}\tilde{I}_2) - \frac{1}{2}\tilde{I}_1} = -\frac{\sqrt{3}(\kappa_1 + 4\sqrt{3}\kappa_2) + 9\kappa_1\alpha_1 - \alpha_2}{\frac{3}{5}(\kappa_1 + \sqrt{3}\kappa_2)\left(-2\alpha_1 + \sqrt{3}\alpha_2\right) - \frac{81}{20}\kappa_1^2 - \frac{9}{5}\kappa_2}. \tag{41}$$

Hence, κ_1 and κ_2 are the free parameters here, where defining $\kappa_{1,2}$ gives us a, b, c, d from (39) and then ω using (41).

As an aside, if the minimum and maximum headway are set to h_{min} and h_{max} respectively, we want solutions with $h_{min} \leq h_c \leq h_{max}$ ($\Delta x_j = h_c + O(\epsilon)$), which suggests $R_{min} \leq 0 \leq R_{max}$ (refer to (6)). This is due to seeking travelling wave solutions that represent disturbances to the steady state of h_c. Consequently, given $u_0 \in [b, c]$ and $R = \sqrt{\omega}(u_0 - 1/\sqrt{3}) + O(\epsilon)$, any solution must have $b \leq 1/\sqrt{3}$ and $c \geq 1/\sqrt{3}$. One way to satisfy both these criteria, from (21b) and (21c), is to set

$$\kappa_2 = \frac{1}{36} - \frac{\kappa_1}{\sqrt{3}}. \tag{42}$$

This gives a definition for κ_2 as a function of κ_1. Using (42) ensures either $b = 1/\sqrt{3}, c > 1/\sqrt{3}$ or $b < 1/\sqrt{3}, c = 1/\sqrt{3}$. As a result, $R \in [0, R_{max}]$ or $R \in [R_{min}, 0]$ respectively. By now restricting our parameter space with (42), the solutions obtained will represent two different scenarios. These correspond to either clusters of cars that move slower or faster than the steady state vehicles travelling with velocity $V(h_c)$, when $R \in [R_{min}, 0]$ or $R \in [0, R_{max}]$ respectively. In particular, we can then highlight solutions that depict traffic congestion by focussing upon the first scenario.

So, finding the four roots of (39) determines the solution parameters a, b, c, d, and then m using (23c), for some given κ_1 and where κ_2 is defined by (42). Hence, a, b, c, d, as well as the wave modulus m are identified as a function of κ_1, which are shown along the top panel of Figure 1. Given this relation between m, a, b, c, d and the parameter κ_1 (also the properties α_1 and α_2 depend upon m, c, d and $e = -(b-d)/(b-c)$), we can then obtain the wave speed (41) as a function of κ_1. This is displayed on the bottom left of Figure 1. It should be noted that the shift θ_0 is arbitrary since it has no influence on the other solution parameters. Therefore, we set $\theta_0 = 0$ for the remainder of the paper.

From the top panel of Figure 1 it is apparent that as $\kappa_1 \to 0.128$, then $m \to 0$ ($b \to c$). Here, there is only one possible solution of $u_0 \to 1/\sqrt{3}$, where the headway tends to the constant state h_c. Furthermore, at the limits of $\kappa_1 \to 0.037, 0.220$ and where $m \to 1$ ($b \to a$ or $c \to d$), the leading order solution u_0 becomes a soliton. More specifically, there are two types of soliton solutions that can be derived from (22). Firstly, (22) must be rewritten in the form

$$u_0 = b + \frac{(c-b)\,\mathrm{cn}^2(\beta\theta; m)}{1 + \frac{1}{e}\,\mathrm{sn}^2(\beta\theta; m)},$$

where cn is a Jacobi elliptic function. Next, by letting $b \to a$ ($m \to 1$, $\kappa_1 \to 0.037$), we find

$$u_0 \to a + \frac{c-a}{\cosh^2 \beta\theta - \frac{a-c}{a-d}\sinh^2 \beta\theta},$$

where $P \to \infty$ (this solution is not periodic), which is referred to as a bright soliton. Conversely, if $c \to d$ ($m \to 1$, $\kappa_1 \to 0.220$), then u_0 reduces to

$$u_0 \to d - \frac{d-b}{\cosh^2 \beta\theta - \frac{d-b}{d-a}\sinh^2 \beta\theta},$$

where $P \to \infty$, which corresponds to a dark soliton. For further details on this analysis, refer to Kamchatnov et al. (2012). Note that since we are concerned with periodic boundaries, we restrict our attention to $m < 1$.

4.1 Periodic boundaries

The parameters of the leading order solution (22) have been defined in terms of the constant κ_1 (see Figure 1). By now using the variables j and t that appear in the traffic model (2) and applying periodic boundary conditions, the connection between this constant and the driver's sensitivity, $\hat{a}$, is also established.

To begin, u_0 is written in terms of j and t by substituting (5) into (22). This gives

$$u_0(j,t) = c + (d-c)\frac{\mathrm{sn}^2\left(\beta k\left(\epsilon(j + V'(h_c)t) - \omega\frac{V'(h_c)}{6}\epsilon^3 t\right); m\right)}{e + \mathrm{sn}^2\left(\beta k\left(\epsilon(j + V'(h_c)t) - \omega\frac{V'(h_c)}{6}\epsilon^3 t\right); m\right)}, \tag{43}$$

where

$$\beta k = \sqrt{\frac{\omega(a-c)(b-d)}{8}}. \tag{44}$$

To ensure this solution satisfies periodic boundary conditions, it is necessary for

$$\frac{2P}{k\epsilon}n = N, \tag{45}$$

where $2P/k\epsilon$ is the period in the j direction and n is some positive integer representing the number of oscillations over the domain $j \in [0, N]$. However, from (23a), it is known

$$\left(\frac{P}{k}\right)^2 = \frac{8K(m)^2}{\omega(a-c)(b-d)}. \tag{46}$$

Therefore, combining (45) and (46), as well as using $\epsilon^2 = (\hat{a}_c/\hat{a}) - 1$, we arrive at

$$\frac{\hat{a}_c}{\hat{a}} = \frac{32K(m)^2n^2}{\omega(a-c)(b-d)N^2} + 1.$$

Rearranging this, a definition for the driver's sensitivity is found, such that

$$\frac{\hat{a}}{\hat{a}_c} = \frac{\hat{a}_c\omega(a-c)(b-d)N^2}{32K(m)^2n^2 + \omega(a-c)(b-d)N^2}. \tag{47}$$

This relation is dependent upon the parameters $n/N, \omega, m, a, b, c, d$.

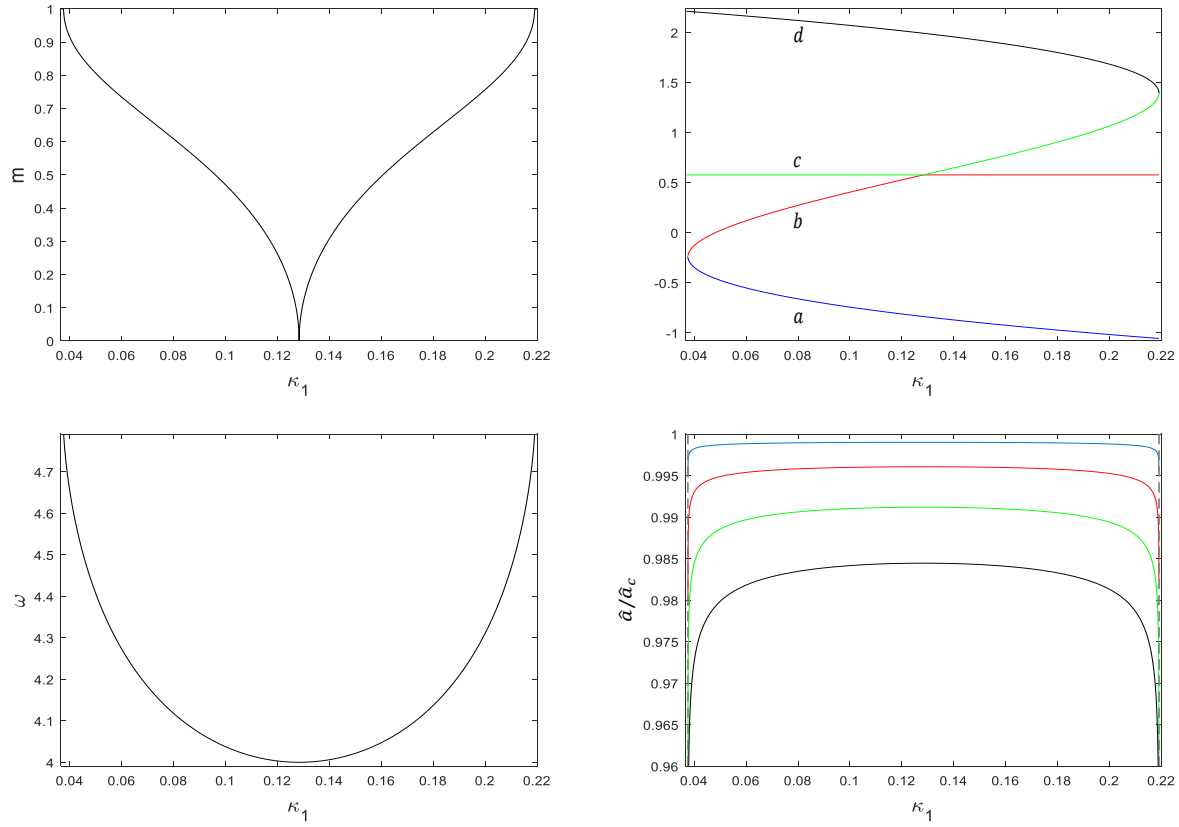

Figure 1: The parameter space for the periodic asymptotic solutions. Top left: The plot of m, (23c), as a function of κ_1. Top right: The plot of a (blue), b (red), c (green), d (black) as a function of κ_1, which are the roots of (39). Bottom left: The plot of ω, (41), as a function of κ_1. Bottom right: The plot of the driver's sensitivity $\hat{a}/\hat{a}_c$, (47), as a function of κ_1, where $N = 100$ and blue: $n = 1$, red: $n = 2$, green: $n = 3$, black: $n = 4$. Defining $\hat{a}/\hat{a}_c$ with (47) ensures periodic boundary conditions are satisfied.

For our fixed point solutions, the relationships between m, a, b, c, d, ω and κ_1 have been obtained (see Figure 1). Using these and (47), $\hat{a}/\hat{a}_c$ as a function of κ_1 is found for some fixed n/N. This relation is plotted on the bottom right of Figure 1 for various n/N values. Note that when (47) holds, the solution will satisfy periodic boundary constraints. By relating $\hat{a}$ to the asymptotic analysis then enables us to compare numerical solutions of the OV system (2) to our solutions.

If $\hat{a}/\hat{a}_c$ and n/N are specified, from the curves shown in Figure 1, the wave modulus m (as well as a, b, c, d) and wave speed ω are identified. Hence, the solution parameters of (43) are defined by choosing $\hat{a}/\hat{a}_c$ and n/N. Moreover, Figure 1 reveals that for some fixed $\hat{a}/\hat{a}_c$ and n/N, there are two possible values for κ_1, and therefore, two valid fixed point solutions. For the remainder of this paper, solutions with $\kappa_1 \lesssim 0.128$ ($\kappa_1 \gtrsim 0.128$) are referred to as the first (second) solution. The first solution represents traffic congestion since it is of a downward form with $u_0 \leq 1/\sqrt{3}$, which means the headway is less than or equal to the critical headway. Whereas, the second solution is of an upward form with $u_0 \geq 1/\sqrt{3}$, which is the inverted counterpart of the downward solution i.e. $R_{up} = -R_{down}$ or $u_{0,up} = -u_{0,down} + 2/\sqrt{3}$.

In Figure 2, left, the maximum and minimum headway exhibited by the upward and downward

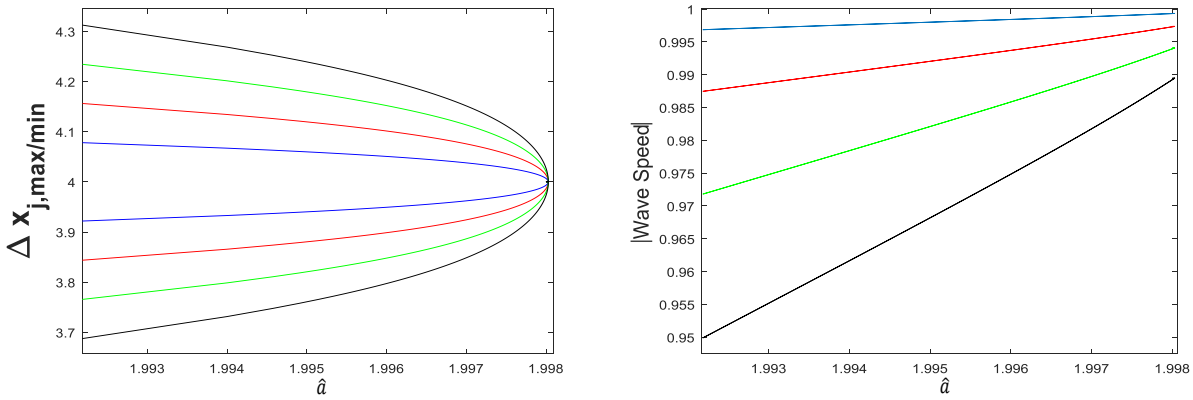

Figure 2: The amplitude and wave speed of our periodic solutions (43), where $h_c = 4$, $N = 100$ and blue: $n = 1$, red: $n = 2$, green: $n = 3$, black: $n = 4$. Left: The maximum (minimum) headway of the upward (downward) solutions. Right: The magnitude of the wave speed in (j, t) space.

solutions respectively are conveyed, when $h_c = 4$ and $n = 1, 2, 3, 4$, as a function of $\hat{a}$. This figure demonstrates that as the driver's sensitivity decreases, the wave amplitude grows, which becomes larger as n is increased. Hence, the size of the disruption to the steady state is greater when $\hat{a}$ is reduced. Also, Figure 2, right reveals the size of the wave speed as a function of $\hat{a}$ in (j, t) space for $h_c = 4$, defined as $V'(h_c) - \omega \frac{V'(h_c)}{6} \epsilon^2$. This shows us that the magnitude of the wave speed grows with $\hat{a}$, which becomes larger when n is reduced. Therefore, the disturbance to the steady state propagates faster when the driver has increased sensitivity.

Thus, a large family of spatially periodic steady travelling waves have been highlighted that do not slowly evolve, where their amplitude, mean height and period remain fixed. This solution type was discussed by Komatsu and Sasa (1995), where it was conjectured that they were always unstable. Note however that a different subspace of the parameter space was considered by Komatsu and Sasa (1995) such that a different restriction was imposed upon κ_1. Furthermore, they did not establish the connection between the driver's sensitivity and the modulation term. Since we have obtained this relationship for our periodic solutions, their numerical stability can now be examined.

5 Stability of Periodic Solutions

The asymptotic spatially periodic headway solutions are now fully defined, such that

$$\Delta x_j(t) = h_c + \epsilon \sqrt{\frac{\omega V'(h_c)}{\mid V'''(h_c) \mid}} \left(u_0(j,t) - \frac{1}{\sqrt{3}} \right), \tag{48}$$

where $u_0(j, t)$ is given by (43). The solution parameters m, a, b, c, d, ω and $\epsilon = \sqrt{(\hat{a}_c/\hat{a}) - 1}$ are established using the steps outlined in Section 4 (also refer to Figure 1). More specifically, from the bottom right plot of Figure 1, choosing $\hat{a}/\hat{a}_c$ and n/N then determines κ_1, which then gives a, b, c, d with (39). Next, m is defined using (23c) and lastly, ω is identified with (41).

The traffic model (2) governing headway is next solved with MATLAB's ode45, where the initial condition for the numerical simulations is defined by (48) when $t = 0$. As well, periodic boundary

conditions are implemented. Then, over different time intervals, the asymptotic and numerical results are compared in Figures 3-6. Here, the number of cars on the road is set to 100. In particular, we analyse the numerical results at t very large to determine if our solutions are numerically stable.

For Figures 3-5, the top panel conveys the asymptotic solution (43) over the domain $j \in [0, 100]$ and $t \in [0, 100]$. The middle panel then compares the asymptotic solution in black to the red-dotted numerical result for $j = 0, 100$, $t \in [0, 100]$ (left) and $j \in [0, 100]$, $t = 10,000$ (right). Lastly, the bottom plot depicts the numerical solution for $j \in [0, 100]$ and $t \in [9600, 10000]$.

The first, downward solution for $h_c = 4$, $\hat{a} = 1.99$ ($\epsilon = 0.0709$), $n = 1$ and $N = 100$ is shown in Figure 3, where $\kappa_1 = 0.037582$. The top panel reveals two distinct zones. These are, a cluster of vehicles with approximate headway $h_{min} < h_c$ represented by the wave trough and a much smaller vehicle cluster with headway h_c corresponding to the wave peak. So, a vehicle travelling at the safety distance h_c decelerates due to a slower preceding vehicle and then endures a prolonged slow period, with approximate headway h_{min}. They then return to the safety distance momentarily to repeat this process. The middle panel of Figure 3 reveals excellent agreement between the two solutions. The numerical result at t very large is examined in the middle and lower panels, where the numerical wave appears to propagate without divergence, a change in amplitude or the development of a phase shift, when compared to the asymptotic solution. This suggests that this spatially periodic solution is stable.

Figure 4 portrays the alternate second solution for $h_c = 4$, $\hat{a} = 1.99$ ($\epsilon = 0.0709$), $n = 1$ and $N = 100$, where $\kappa_1 = 0.219018$. The top panel shows it is of an upward form since now the headway varies between h_c and $h_{max} > h_c$. Therefore, a vehicle travelling at the safety distance h_c will now accelerate as the preceding car is faster. This vehicle then experiences an extended faster state, travelling with the approximate headway h_{max}. Next, they decelerate and revert to the safety distance h_c. The car remains briefly at h_c and then repeats this motion. The middle panel shows again little discrepancy between the asymptotic and numerical solutions. As well, the middle right and bottom figures investigate the long-time behaviour of the numerical result. Once again, no evidence of a phase shift or amplitude variation is exhibited and thus, this solution appears stable.

Next, the driver's sensitivity is reduced to $\hat{a} = 1.98$ and as a result, the perturbation parameter increases to $\epsilon = 0.1005$. The first solution is displayed in Figure 5 where $h_c = 4$, $n = 1$, $N = 100$ and $\kappa_1 = 0.037578$. The vehicle behaviour is consistent with Figure 3, except now the wave trough is flatter and h_{min} has decreased. Hence, the duration of a car travelling with approximate headway h_{min} is longer and the reduction in speed is greater. The middle panel depicts some very small differences between the asymptotic and numerical solutions due to increasing ϵ, although the match is still very good. Analysing the solution at t very large in the middle right and bottom figures, it is apparent that the numerical result is again stable since the phase and amplitude appear constant with increasing t. There is also a second, upward stable solution that corresponds to the parameters $\hat{a} = 1.98$, $h_c = 4$, $n = 1$ and $N = 100$, although it is not depicted here. This solution will have the same behaviour as that conveyed by Figure 4, such that $\Delta x_j \in [h_c, h_{max}]$.

So far, the solutions considered all have one peak/trough over the domain $j \in [0, 100]$, since $n = 1$. Instead, choosing $n > 1$, multiple oscillations over the domain will occur. As an example, the downward solution corresponding to $\hat{a} = 1.99$, $h_c = 4$, $n = 2$, $N = 100$, $\kappa_1 = 0.051638$ is shown in Figure

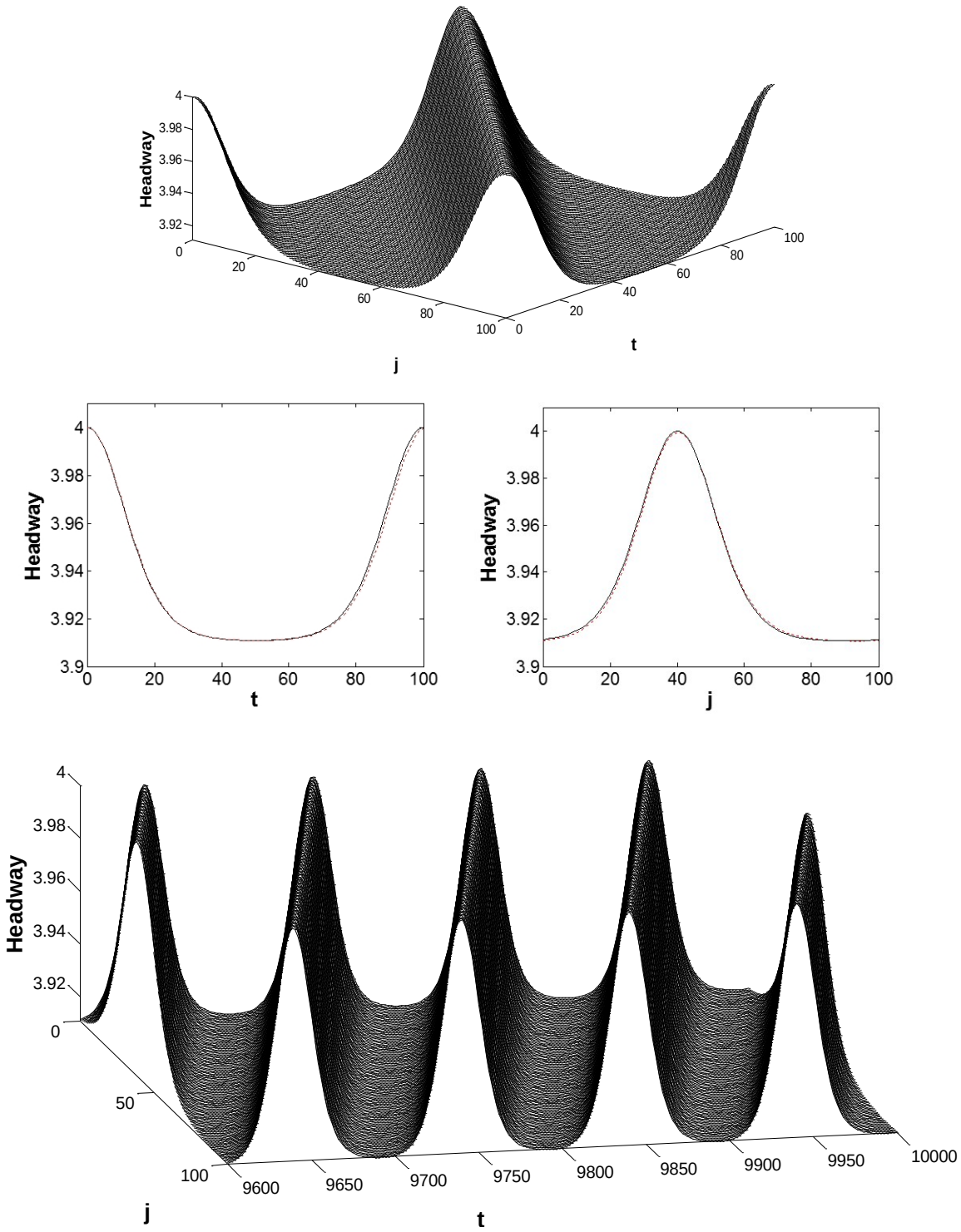

Figure 3: Headway solutions to the model (2) that satisfy periodic boundaries, where $m = 0.99659$, $\epsilon = 0.0709$, $\omega = 4.79$, $\hat{a} = 1.99$, $n = 1$, $N = 100$, $\kappa_1 = 0.037582$. *Top: The asymptotic solution for* $j \in [0, 100]$ *and* $t \in [0, 100]$. *Middle left: The asymptotic solution (black) compared to the numerical solution (red dotted) when* $j = 0, 100$ *and* $t \in [0, 100]$. *Middle right: The asymptotic solution (black) compared to the numerical solution (red dotted) when* $t = 10000$ *and* $j \in [0, 100]$. *Bottom: The numerical solution for* $j \in [0, 100]$ *and* $t \in [9600, 10000]$.

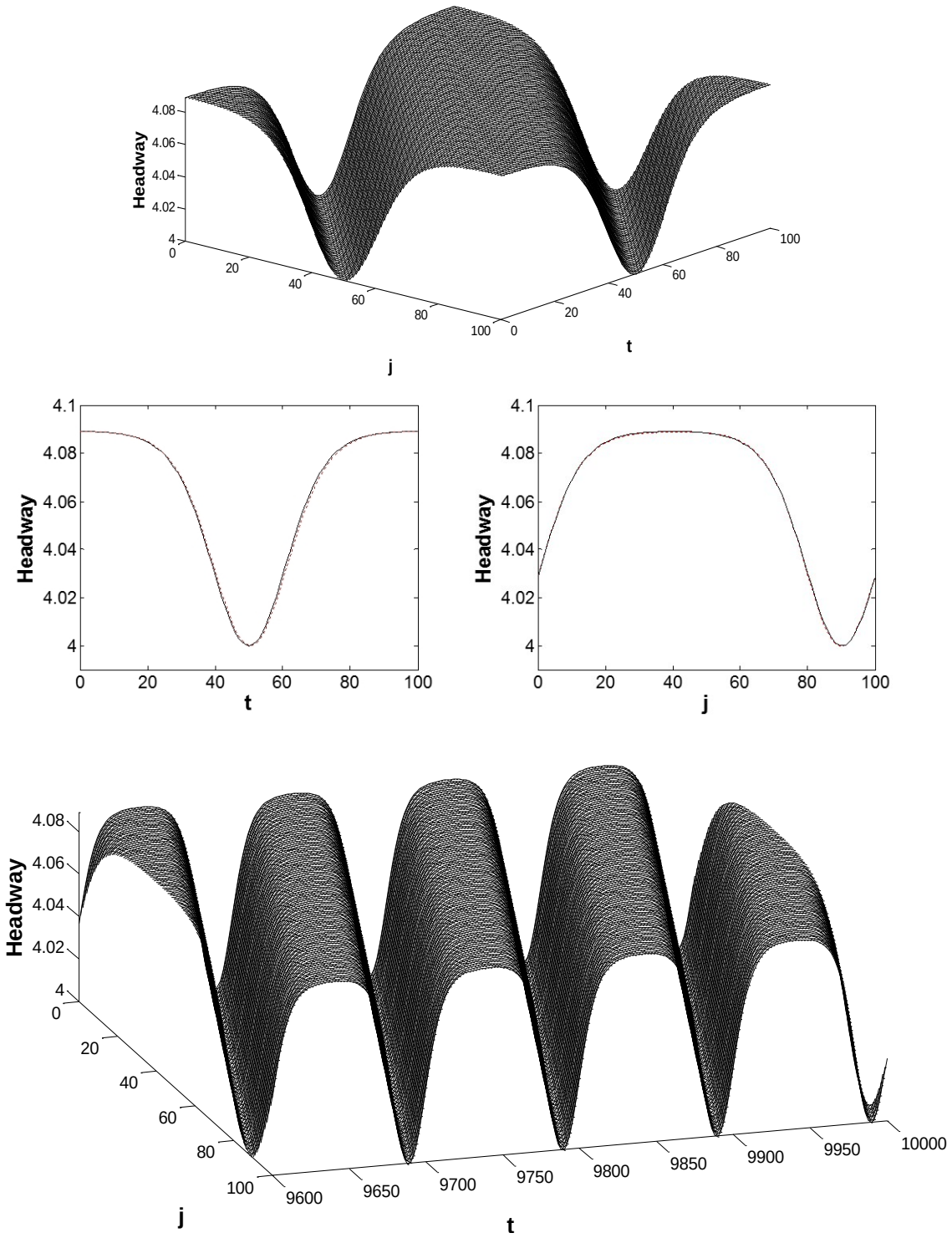

Figure 4: Headway solutions to the model (2) that satisfy periodic boundaries, where $m = 0.99659$, $\epsilon = 0.0709$, $\omega = 4.79$, $\hat{a} = 1.99$, $n = 1$, $N = 100$, $\kappa_1 = 0.219018$. *Top: The asymptotic solution for* $j \in [0, 100]$ *and* $t \in [0, 100]$. *Middle left: The asymptotic solution (black) compared to the numerical solution (red dotted) when* $j = 0, 100$ *and* $t \in [0, 100]$. *Middle right: The asymptotic solution (black) compared to the numerical solution (red dotted) when* $t = 10000$ *and* $j \in [0, 100]$. *Bottom: The numerical solution for* $j \in [0, 100]$ *and* $t \in [9600, 10000]$.

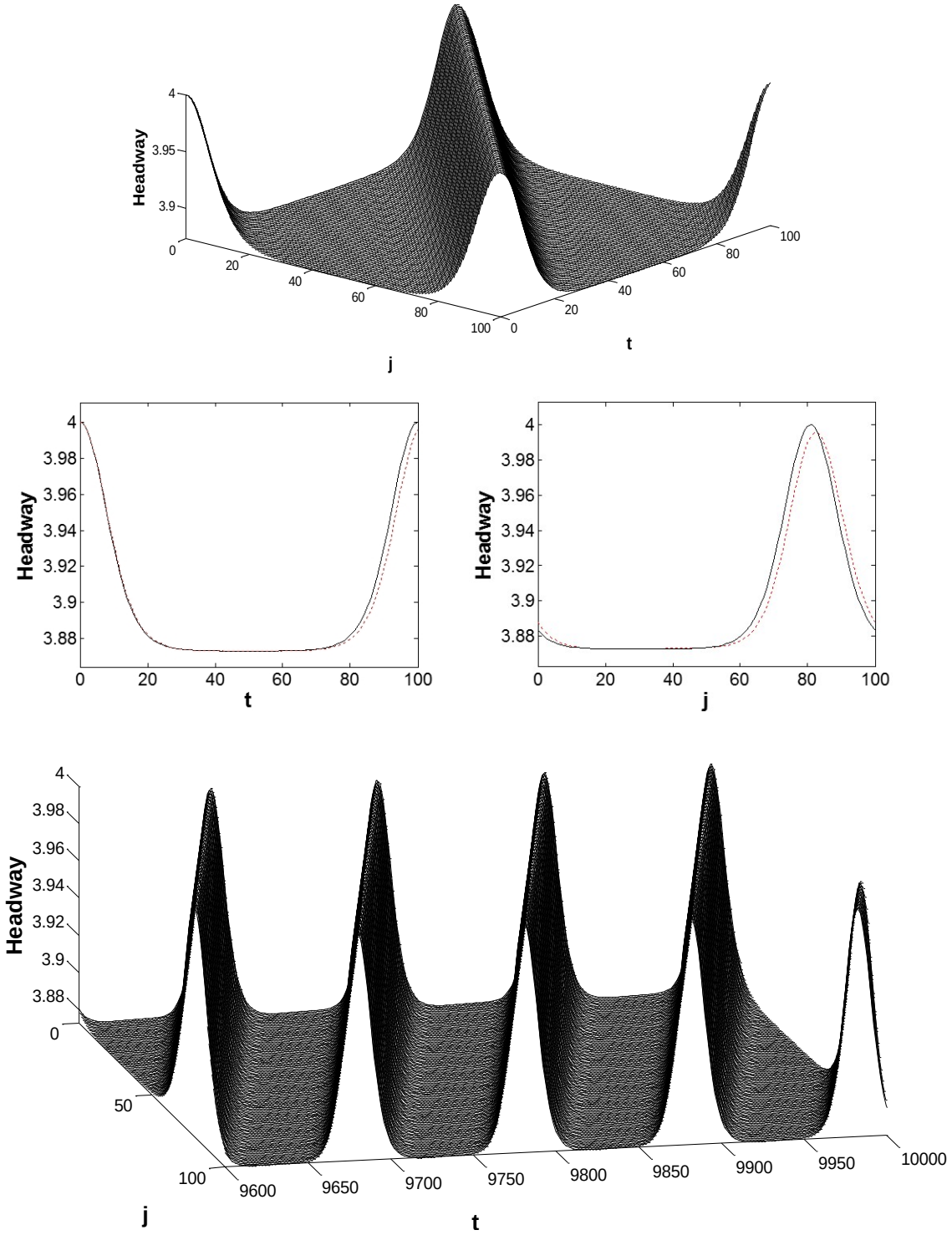

Figure 5: Headway solutions to the model (2) that satisfy periodic boundaries, where $m = 0.99987$, $\epsilon = 0.1005$, $\omega = 4.80$, $\hat{a} = 1.98$, $n = 1$, $N = 100$, $\kappa_1 = 0.037578$. *Top: The asymptotic solution for* $j \in [0, 100]$ *and* $t \in [0, 100]$. *Middle left: The asymptotic solution (black) compared to the numerical solution (red dotted) when* $j = 0, 100$ *and* $t \in [0, 100]$. *Middle right: The asymptotic solution (black) compared to the numerical solution (red dotted) when* $t = 10000$ *and* $j \in [0, 100]$. *Bottom: The numerical solution for* $j \in [0, 100]$ *and* $t \in [9600, 10000]$.

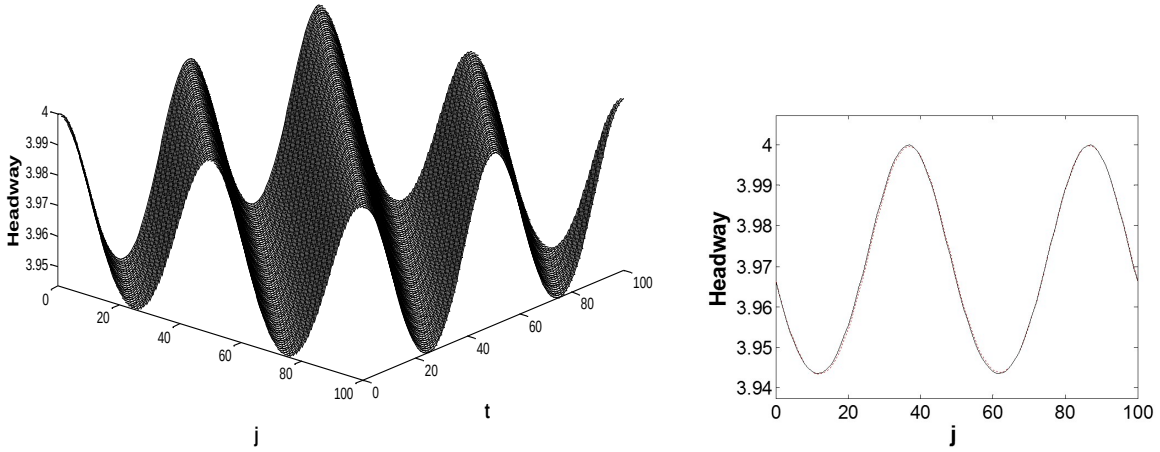

Figure 6: Headway solutions to the model (2) that satisfy periodic boundaries, where $m = 0.792877$, $\epsilon = 0.0709$, $\omega = 4.38$, $\hat{a} = 1.99$, $n = 2$, $N = 100$, $\kappa_1 = 0.051638$. *Left: The asymptotic solution for* $j \in [0, 100]$ *and* $t \in [0, 100]$. *Right: The asymptotic solution (black) compared to the numerical solution (red dotted) when* $t = 10000$ *and* $j \in [0, 100]$.

6. The behaviour observed on the left is consistent with $n = 1$ (Figure 3), except waves with two headway troughs/peaks over $j \in [0, 100]$ now propagate. The long-time dynamics are examined on the right, where the black and red-dotted curves correspond to the asymptotic and numerical solutions respectively when $t = 10000$. The solution appears stable since no phase or amplitude changes are exhibited.

Thus, the long-time dynamics revealed by the numerical results suggest that our set of periodic solutions is stable, although further work is needed to prove this conclusively. Note however that their numerical stability applies only within a certain neighbourhood of the neutral stability line's critical point (see Section 2).

In contrast, Komatsu and Sasa (1995) found solutions of a similar form that they supposed were always unstable, and therefore not observed numerically. More specifically, Komatsu and Sasa (1995) studied solutions of the traffic model (2), which they also reduced to, at leading order,

$$R_{\bar{t}} - R_{\bar{x}\bar{x}\bar{x}} + \left(R^3\right)_{\bar{x}} + O(\epsilon) = 0, \tag{49}$$

using perturbation analysis. Next letting $\tilde{x} = \bar{x} - \omega\bar{t}$ and integrating, (49) becomes

$$-\omega R - R_{\tilde{x}\tilde{x}} + R^3 + O(\epsilon) = C, \tag{50}$$

where C is an integration constant. The equivalent analysis detailed by Komatsu and Sasa (1995) set $C = 0$, which subsequently, in relation to this work, places a different restriction upon κ_1, where $\kappa_1 = (2\sqrt{3})/27$, and κ_2 becomes the free parameter. As a result of these parameter choices, their solutions have a mean height of headway h_c. This means that these solutions characterise two states, which are clusters of vehicles moving at a speed slower and faster than the uniform speed of $V(h_c)$. In contrast, the solutions obtained using (42) describe the two states; vehicle clusters moving with speed $V(h_c)$ and vehicle clusters moving at a speed slower (downward solution)/faster (upward solution) than

$V(h_c)$. Consequently, our waves represent, from the perspective of the driver, a transient but reoccurring disturbance to the steady state of headway h_c.

6 Conclusion

The OV model (2) was used to predict traffic behaviour. In particular, this model's linearly unstable region was studied, where (2) transformed into the mKdV equation with higher order correction terms (see (7)). A multi-scale perturbation method was applied to this equation to locate steady travelling wave solutions, where the travelling wave propagation coordinate was assumed to evolve on a slow and fast scale. Consequently, a leading order solution dependent upon slow and fast variables was defined. A system of differential equations at the next order was also found, which described this solution's slow evolution. The critical points of this system were shown to represent a family of steady travelling waves that had constant amplitude, mean height and period, which represented disturbances to the steady state of headway h_c. Imposing periodic boundary constraints then determined the connection between the solution parameters and the driver's sensitivity, $\hat{a}$, where for some fixed value of $\hat{a}$, two solutions existed of upward and downward form. In particular, the amplitude and speed of the disturbance was obtained as a function of $\hat{a}$. As a result of establishing the relationship between the multi-scale analysis and $\hat{a}$, numerical simulations of the OV model (2) were performed. This validated our analysis by demonstrating excellent agreement between the asymptotic and numerical solutions. Furthermore, we examined the behaviour of these periodic solutions when t was very large. This showed that the numerical waves did not diverge, exhibit any phase shift or variation in amplitude, suggesting that our set of solutions was stable. Hence, steady periodic travelling wave solutions of (7) are observed numerically. Therefore, identifying these solutions will have important implications for future studies of the traffic model (2), particularly when numerically evaluating (2) within the unstable region and interpreting the results.

Appendix

To calculate the integrals $\tilde{I}_i$ (see (32)), first let us define

$$\alpha_1 = \frac{1}{2P}\int_{\theta_1}^{\theta_2} u_0 d\theta, \quad \alpha_2 = \frac{1}{2P}\int_{\theta_1}^{\theta_2} u_0^2 d\theta. \tag{51}$$

These integrals written in full are

$$\alpha_1 = c + \frac{(d-c)}{2P}\int_{\theta_1}^{\theta_2} \frac{\mathrm{sn}^2(\beta(\theta-\theta_0))}{e+\mathrm{sn}^2(\beta(\theta-\theta_0))} d\theta,$$
$$\alpha_2 = c^2 + \frac{2c(d-c)}{2P}\int_{\theta_1}^{\theta_2} \frac{\mathrm{sn}^2(\beta(\theta-\theta_0))}{e+\mathrm{sn}^2(\beta(\theta-\theta_0))} d\theta + \frac{(d-c)^2}{2P}\int_{\theta_1}^{\theta_2} \frac{\mathrm{sn}^4(\beta(\theta-\theta_0))}{\left(e+\mathrm{sn}^2(\beta(\theta-\theta_0))\right)^2} d\theta,$$

given (22). Next, using Byrd and Friedman (1954) to solve these integrals, gives us

$$\begin{aligned}
&\frac{1}{2P}\int_{\theta_1}^{\theta_2}\frac{\mathrm{sn}^2(\beta(\theta-\theta_0))}{e+\mathrm{sn}^2(\beta(\theta-\theta_0))}d\theta = 1-\frac{\Pi(-1/e,m)}{K(m)},\\
&\frac{1}{2P}\int_{\theta_1}^{\theta_2}\frac{\mathrm{sn}^4(\beta(\theta-\theta_0))}{\left(e+\mathrm{sn}^2(\beta(\theta-\theta_0))\right)^2}d\theta\\
&=\frac{1}{K(m)}\left(K(m)-2\Pi(-1/e,m)\right)-\frac{1}{2(1/e+1)}\\
&+\frac{1}{2K(m)(-1/e-1)(m^2+1/e)}\left(-\frac{E(m)}{e}+\Pi(-1/e,m)(-2m^2/e-2/e-1/e^2-3m^2)\right),
\end{aligned}$$

where K, E and Π are the complete elliptic integrals of the first, second and third kind respectively. Therefore, α_1 and α_2 are functions of the solution parameters m, c, d and e (see (22)).

There are a number of steps undertaken to compute the integrals $\tilde{I}_i$ as a function of α_1 and α_2. The following provides a summary of this analysis:

1. Integrate (16) over the domain $\theta\in(\theta_1,\theta_2)$ to obtain the integral $\int_{\theta_1}^{\theta_2}u_0^3d\theta$ in terms of α_1 and α_2.
2. Integrate $u_0\times$(16) and (17) over the domain $\theta\in(\theta_1,\theta_2)$, and then combine, to obtain the integrals $\int_{\theta_1}^{\theta_2}u_0^4d\theta$ and $\int_{\theta_1}^{\theta_2}u_{0,\theta}^2d\theta$ in terms of α_1 and α_2.
3. Integrate $u_0^2\times$(16) and $u_0\times$(17) over the domain $\theta\in(\theta_1,\theta_2)$, and then combine, to obtain the integrals $\int_{\theta_1}^{\theta_2}u_0^5d\theta$ and $\int_{\theta_1}^{\theta_2}u_{0,\theta}^2u_0d\theta$ in terms of α_1 and α_2.
4. Integrate $u_0^3\times$(16) and $u_0^2\times$(17) over the domain $\theta\in(\theta_1,\theta_2)$, and then combine, to obtain the integrals $\int_{\theta_1}^{\theta_2}u_0^6d\theta$ and $\int_{\theta_1}^{\theta_2}u_{0,\theta}^2u_0^2d\theta$ in terms of α_1 and α_2.

As a result, we arrive at

$$\begin{aligned}
\tilde{I}_1&=\frac{1}{\lambda k^2}\left(-\frac{\nu^2}{12\gamma}\alpha_2+\left(\alpha_1+\frac{\nu}{6\gamma}\right)\hat{C}+\frac{4}{3}\hat{D}\right),\\
\tilde{I}_2&=\frac{\gamma}{6\lambda k^2}\left(\alpha_2\left(\frac{9\hat{C}}{2\gamma}-\frac{5\nu^3}{8\gamma^3}\right)+\alpha_1\left(\frac{6\hat{D}}{\gamma}+\frac{3\nu\hat{C}}{2\gamma^2}\right)+\frac{5\nu^2\hat{C}}{4\gamma^3}+\frac{\nu\hat{D}}{\gamma^2}\right),\\
\tilde{I}_3&=\frac{\gamma}{6\lambda k^2}\left(\alpha_2\left(\frac{69\hat{C}\nu}{10\gamma^2}-\frac{7\nu^4}{8\gamma^4}+\frac{24\hat{D}}{5\gamma}\right)+\alpha_1\left(\frac{6\nu\hat{D}}{5\gamma^2}+\frac{21\nu^2\hat{C}}{10\gamma^3}\right)+\frac{35\nu^3\hat{C}}{20\gamma^4}+\frac{7\nu^2\hat{D}}{5\gamma^3}-\frac{54\hat{C}^2}{5\gamma^2}\right).
\end{aligned}$$

Next, the integral $\tilde{I}_4$ can be written, from (14a),

$$\begin{aligned}
\tilde{I}_4=\frac{1}{2P}\int_{\theta_1}^{\theta_2}u_0u_{0,\theta\theta\theta\theta}d\theta&=-\frac{1}{2P}\int_{\theta_1}^{\theta_2}u_{0,\theta}u_{0,\theta\theta\theta}d\theta\\
&=-\frac{1}{2P}\int_{\theta_1}^{\theta_2}u_{0,\theta}\left(\frac{\gamma}{\lambda k^2}u_0^2u_{0,\theta}-\frac{\nu}{\lambda k^2}u_0u_{0,\theta}\right)d\theta\\
&=-\frac{\gamma}{\lambda k^2}\tilde{I}_3+\frac{\nu}{\lambda k^2}\tilde{I}_2.
\end{aligned}$$

Thus, the integral $\tilde{I}$ reduces to (refer to (31))

$$
\begin{aligned}
\tilde{I} &= 3k^2\tilde{I}_1 - \frac{3}{4}k^4\tilde{I}_4 - \frac{3\omega}{2}k^2\left(\tilde{I}_3 - \frac{2}{\sqrt{3}}\tilde{I}_2 + \frac{1}{3}\tilde{I}_1\right) \\
&= 3k^2\tilde{I}_1 - \frac{3}{4}k^4\left(-\frac{\gamma}{\lambda k^2}\tilde{I}_3 + \frac{\nu}{\lambda k^2}\tilde{I}_2\right) - \frac{3\omega}{2}k^2\left(\tilde{I}_3 - \frac{2}{\sqrt{3}}\tilde{I}_2 + \frac{1}{3}\tilde{I}_1\right) \\
&= k^2\tilde{I}_1\left(3 - \frac{\omega}{2}\right) + k^2\tilde{I}_2\left(-\frac{3\nu}{4\lambda} + \sqrt{3}\omega\right) + 3k^2\tilde{I}_3\left(\frac{\gamma}{4\lambda} - \frac{\omega}{2}\right).
\end{aligned}
$$

References

M. Bando, K. Hasebe, A. Nakayama, A. Shibata, and Y. Sugiyama. Dynamical model of traffic congestion and numerical simulation. *Phys. Rev. E*, 51:1035–1042, 1995.

L. Brillouin. La mécanique ondulatoire de Schrödinger une méthod générale de résolution par approximations successives. *Comptes Rendus Acad. Sci.*, 183:24–26, 1926.

P. Byrd and M. Friedman. *Handbook of Elliptic Integrals for Engineers and Physicists*. Springer-Verlag, Berlin, 1954.

C.F. Daganzo. Requiem for second-order fluid approximations of traffic flow. *Transport Res. B-Meth.*, 29(4):277–286, 1995.

H.X. Ge, R.J. Cheng, and S.Q. Dai. KdV and kink-antikink solitons in car-following models. *Physica A*, 357(34):466–476, 2005.

L. Hattam. KdV cnoidal waves in a traffic flow model with periodic boundaries. *Physica D*, 348:44–53, 2017.

L.L. Hattam and S.R. Clarke. Modulation theory for the steady forced KdV-Burgers equation and the construction of periodic solutions. *Wave Motion*, 56:67–84, 2015.

A.M. Kamchatnov, Y.-H. Kuo, T.-C. Lin, T.-L. Horng, S.-C. Gou, R. Clift, G.A. El, and R.H.J. Grimshaw. Undular bore theory for the Gardner equation. *Phys. Rev. E*, 86:036605–036627, 2012.

S. Katz, J.L. Lebowitz, and H. Spohn. Phase transitions in stationary nonequilibrium states of model lattice systems. *Phys. Rev. B*, 28:1655–1658, 1983.

S. Katz, J.L. Lebowitz, and H. Spohn. Nonequilibrium steady states of stochastic lattice gas models of fast ionic conductors. *J. Stat. Phys.*, 34(3):497–537, 1984.

T.S. Komatsu and S. Sasa. Kink soliton characterizing traffic congestion. *Phys. Rev. E*, 52:5574–5582, 1995.

H.A. Kramers. Wellenmechanik und halbzahlige Quantisierung. *Z. Phys.*, 39(10-11):828–840, 1926.

Z. Li, R. Zhang, S. Xu, and Y. Qian. Study on the effects of driver's lane-changing aggressiveness on traffic stability from an extended two-lane lattice model. *Commun. Nonlinear Sci. Numer. Simul.*, 24(1-3):52–63, 2015.

M.J. Lighthill and G.B. Whitham. On kinematic waves. II. A theory of traffic flow on long crowded roads. *Proc. Roy. Soc. London A*, 229(1178):317–345, 1955.

M. Muramatsu and T. Nagatani. Soliton and kink jams in traffic flow with open boundaries. *Phys. Rev. E*, 60:180–187, 1999.

S. Myint and R. Grimshaw. The modulation of nonlinear periodic wave-trains by dissipative terms in the Korteweg-de Vries equation. *Wave Motion*, 22(2):215–238, 1995.

T. Nagatani. The physics of traffic jams. *Rep. Prog. Phys.*, 65(9):1331, 2002.

G.F. Newell. Nonlinear effects in the dynamics of car following. *Oper. Res.*, 9(2):209–229, 1961.

P.I. Richards. Shock waves on the highway. *Oper. Res.*, 4(1):42–51, 1956.

Y.-Q. Wang, R. Jiang, A.B. Kolomeisky, and M.-B. Hu. Bulk induced phase transition in driven diffusive systems. *Sci. Rep.*, 4(5459), 2014.

G. Wentzel. Eine verallgemeinerung der quantenbedingungen für die zwecke der wellenmechanik. *Z. Phys.*, 38(6-7):518–529, 1926.

H.M. Zhang. A theory of nonequilibrium traffic flow. *Transport Res. B-Meth.*, 32(7):485–498, 1998.

L.-J. Zheng, C. Tian, D.-H. Sun, and W.-N. Liu. A new car-following model with consideration of anticipation driving behavior. *Nonlinear Dyn.*, 70(2):1205–1211, 2012.

H.B. Zhu and S.Q. Dai. Numerical simulation of soliton and kink density waves in traffic flow with periodic boundaries. *Physica A*, 387(16-17):4367–4375, 2008.